NASA/TM—2003-212185

Mode I, Mode II, and Mixed-Mode Fracture of Plasma-Sprayed Thermal Barrier Coatings at Ambient and Elevated Temperatures

Sung R. Choi
Ohio Aerospace Institute, Brook Park, Ohio

Dongming Zhu
U.S. Army Research Laboratory, Glenn Research Center, Cleveland, Ohio

Robert A. Miller
Glenn Research Center, Cleveland, Ohio

March 2003

The NASA STI Program Office . . . in Profile

Since its founding, NASA has been dedicated to the advancement of aeronautics and space science. The NASA Scientific and Technical Information (STI) Program Office plays a key part in helping NASA maintain this important role.

The NASA STI Program Office is operated by Langley Research Center, the Lead Center for NASA's scientific and technical information. The NASA STI Program Office provides access to the NASA STI Database, the largest collection of aeronautical and space science STI in the world. The Program Office is also NASA's institutional mechanism for disseminating the results of its research and development activities. These results are published by NASA in the NASA STI Report Series, which includes the following report types:

- TECHNICAL PUBLICATION. Reports of completed research or a major significant phase of research that present the results of NASA programs and include extensive data or theoretical analysis. Includes compilations of significant scientific and technical data and information deemed to be of continuing reference value. NASA's counterpart of peer-reviewed formal professional papers but has less stringent limitations on manuscript length and extent of graphic presentations.

- TECHNICAL MEMORANDUM. Scientific and technical findings that are preliminary or of specialized interest, e.g., quick release reports, working papers, and bibliographies that contain minimal annotation. Does not contain extensive analysis.

- CONTRACTOR REPORT. Scientific and technical findings by NASA-sponsored contractors and grantees.

- CONFERENCE PUBLICATION. Collected papers from scientific and technical conferences, symposia, seminars, or other meetings sponsored or cosponsored by NASA.

- SPECIAL PUBLICATION. Scientific, technical, or historical information from NASA programs, projects, and missions, often concerned with subjects having substantial public interest.

- TECHNICAL TRANSLATION. English-language translations of foreign scientific and technical material pertinent to NASA's mission.

Specialized services that complement the STI Program Office's diverse offerings include creating custom thesauri, building customized databases, organizing and publishing research results . . . even providing videos.

For more information about the NASA STI Program Office, see the following:

- Access the NASA STI Program Home Page at ***http://www.sti.nasa.gov***

- E-mail your question via the Internet to help@sti.nasa.gov

- Fax your question to the NASA Access Help Desk at 301–621–0134

- Telephone the NASA Access Help Desk at 301–621–0390

- Write to:
  NASA Access Help Desk
  NASA Center for AeroSpace Information
  7121 Standard Drive
  Hanover, MD 21076

NASA/TM—2003-212185

Mode I, Mode II, and Mixed-Mode Fracture of Plasma-Sprayed Thermal Barrier Coatings at Ambient and Elevated Temperatures

Sung R. Choi
Ohio Aerospace Institute, Brook Park, Ohio

Dongming Zhu
U.S. Army Research Laboratory, Glenn Research Center, Cleveland, Ohio

Robert A. Miller
Glenn Research Center, Cleveland, Ohio

Prepared for the
Eighth International Symposium on Fracture Mechanics of Ceramics
sponsored by the University of Houston
Houston, Texas, February 25–28, 2003

National Aeronautics and
Space Administration

Glenn Research Center

March 2003

This report is a formal draft or working paper, intended to solicit comments and ideas from a technical peer group.

Trade names or manufacturers' names are used in this report for identification only. This usage does not constitute an official endorsement, either expressed or implied, by the National Aeronautics and Space Administration.

Available from

NASA Center for Aerospace Information
7121 Standard Drive
Hanover, MD 21076

National Technical Information Service
5285 Port Royal Road
Springfield, VA 22100

Available electronically at http://gltrs.grc.nasa.gov

MODE I, MODE II, AND MIXED-MODE FRACTURE OF PLASMA-SPRAYED THERMAL BARRIER COATINGS AT AMBIENT AND ELEVATED TEMPERATURES

Sung R. Choi
Ohio Aerospace Institute
Brook Park, Ohio 44142

Dongming Zhu
U.S. Army Research Laboratory
Glenn Research Center
Cleveland, Ohio 44135

Robert A. Miller
National Aeronautics and Space Administration
Glenn Research Center
Cleveland, Ohio 44135

The mixed-mode fracture behavior of plasma-sprayed ZrO_2-8 wt% Y_2O_3 thermal barrier coatings was determined in air at 25 and 1316 °C in asymmetric four-point flexure with single edge v-notched beam (SEVNB) test specimens. The mode I fracture toughness was found to be $K_{Ic} = 1.15 \pm 0.07$ and 0.98 ± 0.13 MPa $\sqrt{m}$, respectively, at 25 and 1316 °C. The respective mode II fracture toughness values were $K_{IIc} = 0.73 \pm 0.10$ and 0.65 ± 0.04 MPa $\sqrt{m}$. Hence, there was an insignificant difference in either K_{Ic} or K_{IIc} between 25 and 1316 °C for the coating material, whereas there was a noticeable distinction between K_{Ic} and K_{IIc}, resulting in $K_{IIc}/K_{Ic} = 0.65$ at both temperatures. The empirical mixed-mode fracture criterion best described the coatings' mixed-mode fracture behavior among the four mixed-mode fracture theories considered. The angle of crack propagation was in reasonable agreement with the minimum strain energy density criterion. The effect of the directionality of the coating material in on K_{Ic} was observed to be insignificant, while its sintering effect at 1316 °C on K_{Ic} was significant.

1. INTRODUCTION

Thermal barrier coatings (TBCs) have attracted increasing attention for advanced gas turbine and diesel engine applications due to their ability to provide thermal insulation to engine components.[1–3] The merits of using the ceramic thermal barrier coatings are well recognized and include the potential increase in engine operating temperature with reduced cooling requirements, resulting in significant improvement in thermal efficiency, performance, and reliability. Plasma-sprayed zirconia-based ceramics are one of the most important coating materials in light of their low thermal conductivity, relatively high thermal expansivity, and unique microstructure as a result of the plasma spraying process.

However, the limited durability of thermal barrier coatings under severe thermal and mechanical loading conditions encountered in heat engines remains one of the major problems. As a result, the development of thermal barrier coatings requires a better understanding of both thermal and mechanical behavior of the coating materials to ensure life and reliability of the related components.

It has been suggested that the important limiting factor encountered in thin plasma-sprayed thermal barrier coatings is the relatively low fracture energy of the coating in planes close to and parallel to the interface. Various efforts have been made to determine mode I 'interfacial' fracture toughness of the coatings in the vicinity of the interface using various techniques such as the indentation method, debonding technique, three- or four-point flexure delamination technique, and compact tension test method.[4–6] Failure of the thick thermal barrier coatings has been observed within the bulk of the coating material, independent of any delamination that typically occurs at the interface of a thin coating and a substrate.[7] There have been efforts to determine mode I fracture toughness of thick thermal barrier coatings at ambient and elevated temperatures. In fact, the majority of data on fracture toughness of both thin and thick coating materials have been determined under mode I loading. However, rarely are structural components or coatings subject to pure mode I loading. This is particularly true for thermal barrier coatings that encounter complex thermal and mechanical loading in engine operations. Recently, Callus and Berndt[8] used a pure-shear technique to determine the interfacial critical mode II strain energy release rate of some thin coatings. Their data, however, were only for *ambient* temperature. Mixed-mode data on either thin or thick coatings are rarely available in the literature at *elevated* temperatures, despite an important fact that mechanical behavior of coating materials should not be based solely on ambient-temperature properties. Dense oxide ceramics (such as zirconia) have exhibited significant changes in mechanical properties such as strength, fracture toughness, and slow crack growth when temperature is increased above 800 to 1000 °C.[9]

The objective of this work was to determine modes I and II fracture toughness and mixed-mode fracture behavior of free-standing thermal barrier coatings of plasma-sprayed ZrO_2-8 wt% Y_2O_3 at an *elevated* temperature of 1316 °C in air. The choice of this temperature was based on a typical target temperature of aerospace gas turbine applications. These same properties were also determined at ambient temperature (25 °C). An asymmetric four-point flexure test technique was used at both temperatures in conjunction with single-edge-v-notched beam (SEVNB) test specimens, which yielded simplicity in both specimen and crack preparation and in test procedure. Fracture locus, ranging from mode I to mode II, was determined. Several mixed-mode fracture criteria were analyzed based on experimental data on mode I and mode II stress intensity factors as well as on crack propagation angles. The mixed-mode fracture behavior of the coatings was compared with that of typical advanced structural ceramics in terms of mixed-mode fracture theories. The effects of sintering and the material's directionality on mode I fracture toughness at ambient temperature were also characterized.

2. EXPERIMENTAL PROCEDURES

2.1. Material

The ZrO_2-8 wt% Y_2O_3 powder with an average particle size of 60 μm was first plasma-sprayed on a graphite substrate measuring 150 by 100 by 6.5 mm to a thickness of about 6 mm, using a Sulzer-Metco ATC-1 plasma coating system with an industrial robot. The plasma-spray conditions can be found elsewhere.[10] A free standing, plasma-sprayed ceramic billet was then obtained by burning away the graphite substrate at 680 °C in air for 24 h. The billet was machined into the final, rectangular flexure test specimen with nominal dimensions of 3 by 4 by 50 mm, respectively, in width, depth, and length. The 3-mm-wide face of flexure test specimens corresponded to the plane perpendicular to the plasma spraying direction. Major physical and mechanical properties of as-sprayed coating material including hardness, fracture toughness, and strength have been determined previously at ambient temperature[11, 12] and are presented in Table 1. Figure 1 shows a typical fracture surface and a polished surface showing the microstructure of as-processed coatings, in which large amounts of microcracks and pores are characterized in conjunction with a unique platelet structure.

2.2. Mixed-Mode Fracture Testing

2.2.1. Preparation of sharp precracks

Sharp v notches were introduced in flexure test specimens, using the single-edge-v-notched-beam method.[13] This method utilizes a razor blade with diamond paste to introduce a sharp root radius by tapering a saw cut. Sharp v-notch radii ranging from 4 to 6 μm have been successfully obtained for alumina, glass ceramic, silicon nitride, zirconia, and silicon carbide ceramics.[13] A starter straight-through notch 0.6 mm deep and 0.026 mm wide was made on the 3-mm-wide face of the test specimens. A steel razor blade was put into the starter notch sprinkled with diamond paste with a particle size of 9 μm. Typically, a load of about 10 N was applied through the razor blade with a stroke

Table 1. Typical Physical and Mechanical Properties of Plasma-Sprayed Zro_2-8 Wt% Y_2o_3 Thermal Barrier Coatings at Ambient Temperature[11, 12]

Density, g/cm^3	Elastic modulus[a] (in compression), *E*, GPa	Fracture toughness,[b] K_{Ic}, MPa $\sqrt{m}$	Strength		
			Type of test	Number of specimens	Average strength,[b] MPa
5.22	34	1.0(0.1)	Tension	10	10 (2)
			Trans-thickness tension	10	11(1)
			compression	10	324(72)
			Four-point flexure	20	32(6)
			Biaxial flexure	10	40(4)

[a]The value of *E* is estimated from the starting point of the stress-strain curve.[11]
[b]The number in parenthesis represents the ±1.0 standard deviation.

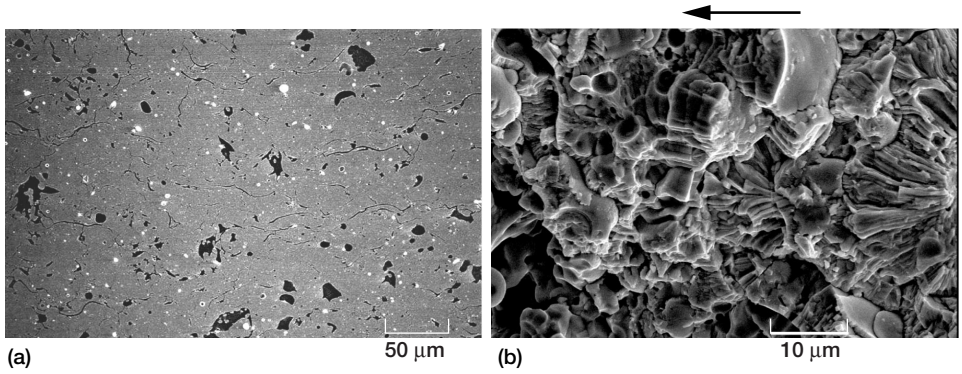

Figure 1.—Typical microstructures of plasma-sprayed ZrO_2-8 wt% Y_2O_3 thermal barrier coatings. (a) Polished surface. (b) Fracture surface. Arrow indicates plasma-spray direction.

rate (back-and-forth motion) of 1 Hz and a stroke distance of about 13 mm in a specially designed polishing machine.[11] The final notch depth and root radius were 2.0 mm and 20 to 50 μm, respectively, resulting in the crack size-to-specimen depth ratio of 0.5 (=a/W). The coating material resulted in less sharpness in root radius due to its porous and microcracked nature, compared to typical dense ceramics. However, it has observed that the sharpness ranging from 20 to 50 μm was sufficient to give a consistent and accurate value of fracture toughness of the coating material.[11] Note that the through-the-thickness sharp notches thus prepared were aligned parallel with respect to the plasma spraying direction.

Other methods to generate sharp cracks to estimate fracture toughness, such as the single-edge-precracked-beam (SEPB)[14] and the indentation techniques, were not feasible for the coating material: The indentation response was poor because of the material's significant porosity, microcracks, and 'softness,' so that well-defined indentation cracks were not achieved. This indicates that microindentation techniques may not be appropriate for plasma-sprayed coating materials whose pore and microcrack sizes in some cases are much greater than microindentation cracks, and as a result, a continuum approach is no longer valid.[11] Also note that cracks produced by this SEVNB method were very uniform in their crack-front geometry and very consistent in size with high reproducibility from specimen to specimen. This gives rise to very little scatter in or a small coefficient of variation in the values of fracture toughness, a notable advantage of the SEVNB method over other methods.

2.2.2. Asymmetric four-point flexure testing

The sharp v-notched flexure test specimen was loaded in asymmetric four-point flexure as shown in figure 2. The ratio of mode I to mode II stress intensity factor (SIF), K_I/K_{II}, was varied by varying the distance of the precrack from the center plane, s, as shown in the figure. When the precrack was centered with respect to the loading point (s = 0), the precrack was subjected to pure mode II loading. As s was increased, K_I/K_{II} also increased. The stress intensity factors, K_I and K_{II}, are expressed as

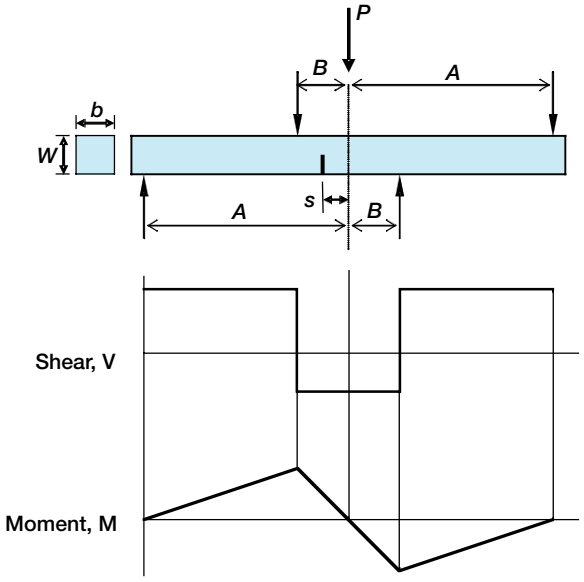

Figure 2.—Schematic of asymmetric four-point flexure geometry with accompanying shear force and bending moment diagrams.

$$K_{\mathrm{I}} = \sigma(\pi a)^{1/2} F_{\mathrm{I}}\left(\frac{a}{W}\right) \tag{1}$$

$$K_{\mathrm{II}} = \tau(\pi a)^{1/2} F_{\mathrm{II}}\left(\frac{a}{W}\right) \tag{2}$$

where σ is the applied (remote) normal stress, τ is the applied (remote) shear stress, a is the crack size, and W is the specimen depth. F_{I} and F_{II} are crack geometry factors in modes I and II, respectively. The normal and shear stresses are given from the elementary beam theory by

$$\sigma = \frac{A - B}{A + B}\left(\frac{6sP}{bW^2}\right) \tag{3}$$

$$\tau = \frac{A - B}{A + B}\left(\frac{P}{bW}\right) \tag{4}$$

where A and B are distances from a load point as defined in figure 2, b is the specimen width, and P is the applied force. The values of A = 10 mm and B = 5 mm were typically used, but in some cases (K_{IIc} at RT) values of A = 12 and B = 6 mm were used for comparison and verification. The test specimen's cross section was W = 4 mm and b = 3 mm.

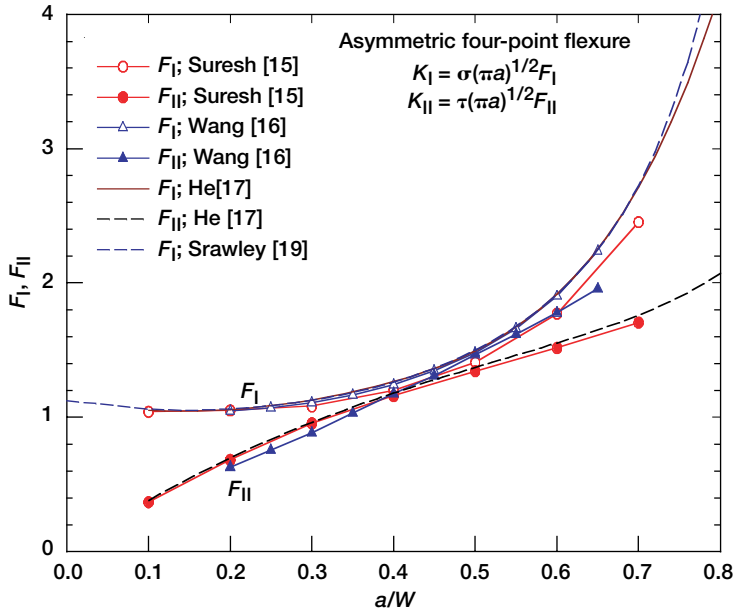

Figure 3.—Various solutions of crack geometry factors F_I and F_{II} applied in the asymmetric four-point flexure configuration.

Several different expressions of F_I and F_{II} were suggested by Suresh et al.,[15] Wang et al.,[16] and He and Hutchinson[17] for the case of through-the-thickness crack, and their respective results of F_I and F_{II} are illustrated in figure 3. As seen from the figure, no significant difference in F_I and F_{II} between the solutions was found, particularly when a/W is between 0.35 and 0.50. The solution by He and Hutchinson[17] that provided a convenient polynomial expression was used in here, and is given as follows:

$$F_I\left(\frac{a}{W}\right) = 1.122 - 1.121\left(\frac{a}{W}\right) + 3.740\left(\frac{a}{W}\right)^2 + 3.873\left(\frac{a}{W}\right)^3 - 19.05\left(\frac{a}{W}\right)^4 + 22.55\left(\frac{a}{W}\right)^5 \quad \text{for} \quad \frac{a}{W} \le 0.7 \tag{5}$$

$$F_{II}\left(\frac{a}{W}\right) = 7.264 - 9.37\left(\frac{a}{W}\right) + 2.74\left(\frac{a}{W}\right)^2 + 1.87\left(\frac{a}{W}\right)^3 - 1.04\left(\frac{a}{W}\right)^4 \quad \text{for} \quad 0 \le \frac{a}{W} \le 1 \tag{6}$$

Note that Eq. (5) was quoted from Murakami's[18] and was almost identical to Srawly and Gross' solution[19] up to $a/W = 0.7$, as seen in the figure. Also note that the difference in F_I and F_{II} between solutions in the range of $a/W = 0.4$ to 0.5 was negligible, resulting in

$$F_{\mathrm{I}} \approx F_{\mathrm{II}} \tag{7}$$

Hence, in the case of a/W = 0.4 to 05, the $K_{\mathrm{II}}/K_{\mathrm{I}}$ ratio (or called 'mixity') can be simplified from Eqs. (1)–(4) and (7) as follows:

$$\frac{K_{\mathrm{II}}}{K_{\mathrm{I}}} = \frac{WF_{\mathrm{II}}}{6sF_{\mathrm{I}}} \approx \frac{W}{6s} \tag{8}$$

$$\beta = \tan^{-1}\left(\frac{K_{\mathrm{II}}}{K_{\mathrm{I}}}\right) \approx \tan^{-1}\left(\frac{W}{6s}\right) \tag{9}$$

where β is the mixity angle. The angle β was also called the "equivalent crack angle" by Maccagno and Knott[20] for situations which do not actually use the inclined crack configuration. The ratio of crack size to specimen width used in this work was chosen to be a/W = 0.5 so that Eq. (8) or (9) could be conveniently used. The values of s = 0 to 3.6 mm were selected to give uniformly distributed β between pure mode I (β = 0°) and pure mode II (β = 90°) based on Eq. (9). Pure mode I fracture toughness K_{Ic} was determined using a symmetric four-point flexure fixture with 10-mm inner and 20-mm outer distances.

All testing was performed in displacement control using a SiC flexure fixture with an actuator speed of 0.5 mm/min of an Instron electromechanical test frame (Model 8562, Instron, Canton, MA). Testing was conducted at 25 and 1316 °C in air. Each test specimen in elevated-temperature testing was held for thermal equilibration for about 20 min prior to testing. At room temperature, four and nine specimens were tested for K_{Ic} and K_{IIc}, respectively, whereas at 1316 °C, four specimens were examined for each test. There were nine mixity values associated with the specimens tested at 25 °C, and four mixity values associated with those tested at 1316 °C. Typically, two or three specimens of each mixity value were tested. After testing, the crack size of each tested specimen was determined optically from its fracture surface based on the three-point measurements in accordance with test standard ASTM C1421.[14] The crack propagation angles were also determined.

2.3. Effects of Sintering and Material Directionality

In order to determine the effect of sintering on mode I fracture toughness of the coating material, additional fracture toughness testing was carried out at ambient temperature using the test specimens annealed at 1316 °C in air for 5, 20, 100, and 500 h. The sharp v-notches were introduced in the annealed specimens using the same technique described in section 2.2.1. The test fixture, test frame, and test procedure used were the same as those used in the aforementioned 'regular' fracture toughness testing. Fracture surfaces were also examined via SEM with respect to annealing time to see any change in microstructure and morphology.

Mode I fracture toughness (K_{Ic}) of as-sprayed coating material was also evaluated at ambient temperature in the plane perpendicular to the plasma-sprayed direction (that is, within the 'layered' direction) using the double cantilever beam (DCB) method. A sharp v notch was introduced in the center plane of the 4-mm-wide face of each flexure test

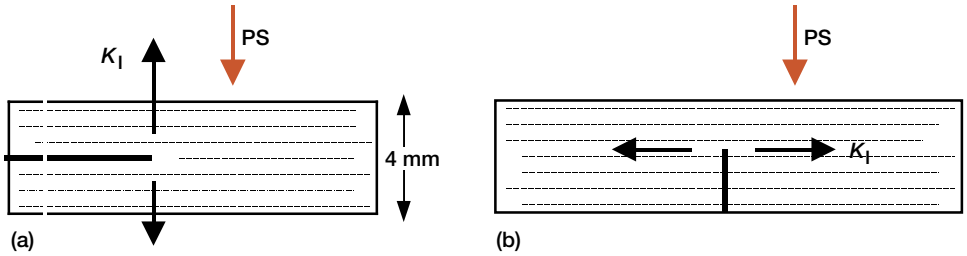

Figure 4.—(a) A schematic geometry of double-cantilever-beam (DCB) test specimens used to determine K_{Ic} in the plane perpendicular to the plasma-sprayed (PS) direction. (b) 'Regular' fracture toughness testing by the SEVNB method with crack planes parallel to the plasma-spraying direction is shown for comparison.

specimen with a crack length of about 6 mm (see fig. 4). Fracture toughness was calculated based on the formula by Murakami.[18] A total of three DCB specimens were tested. This additional fracture testing was to determine directionality of the material in response to fracture toughness relative to the plasma-spraying direction.

3. RESULTS AND DISCUSSION

3.1. Test Results

The results of the mode I, mode II, and mixed-mode fracture testing for the coating material at both 25 and 1316 °C are presented as K_{II} versus K_I in figure 5. Each point represents a single datum, and the values K_{Ic} and K_{IIc} represent the average of four and eight measurements, respectively, at 25 °C and the average of four measurements for each at 1316 °C. The effect of test distance on K_{IIc} at 25 °C was found to be insignificant: K_{IIc} = 0.74±0.1 and 0.69±0.09 MPa$\sqrt{\text{m}}$, respectively, for A/B values of 10/5 and 12/6 mm (see fig. 2). Hence, the 10/5-mm distances were exclusively used throughout the mixed-mode test program. At 25 °C, K_{Ic} = 1.15±0.07 and K_{IIc} = 0.73±0.10 MPa$\sqrt{\text{m}}$, and at 1316 °C, K_{Ic} = 0.98±0.13 and K_{IIc} = 0.65±0.04 MPa$\sqrt{\text{m}}$. Note that the values of K_{IIc} were 37 and 34 percent lower than those of K_{Ic} at 25 and 1316 °C, respectively. It has been reported that for some dense ceramics K_{IIc} was greater than K_{Ic}, presumably attributed to the frictional interaction between the two crack planes.[21] However, the previous studies on advanced (dense) ceramics including silicon nitrides, alumina and zirconia[22, 23] showed a different result that K_{IIc} was almost identical to K_{Ic} for a given material, indicative of an insignificant frictional effect on K_{IIc} by either coarse grained or fine grained ceramics. The coating material, however, did not exhibit a similar value in both K_{IIc} and K_{Ic} but rather yielded a lower value in K_{IIc} than in K_{Ic} at both 25 and 1316 °C. It is believed that because of the porous, microcracked, 'soft' nature the coating material, there would not have been any significant frictional contribution to K_{IIc}. Furthermore, the coating material would be easier to shear (mode II) than to cleave (mode I), probably because of its unique platelet structure formed by plasma-spraying process, which results in low K_{IIc} compared with K_{Ic}. The difference between K_{IIc} and K_{Ic}

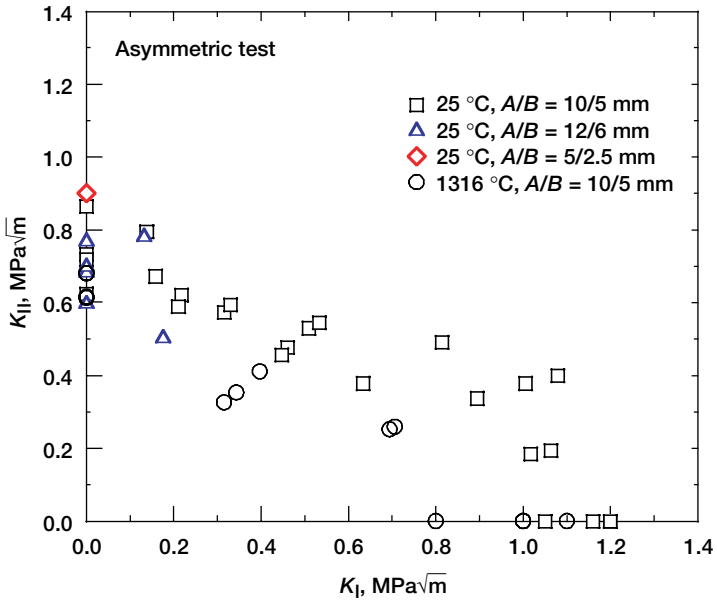

Figure 5.—A summary of K_{II} versus K_I for mode I, mode II, and mixed-mode fracture of plasma-sprayed ZrO_2-8 wt% Y_2O_3 thermal barrier coatings at both 25 and 1316 °C in air.

for various ceramics and brittle materials will be described in more detail in a next section.

As shown in figure 5, because $K_{IIc} < K_{Ic}$, the overall K_{II} versus K_I relation is represented by an ellipse at either 25 or 1316 °C with K_{Ic} being a major axis. For a given mixity angle ranging from $\beta = 0$ to 90°, K_{EQ} [$= (K_I^2+K_{II}^2)^{1/2}$] was lower at 1316 °C than at 25 °C, probably because of a somewhat softening effect at elevated temperature. The values of K_{Ic} and K_{IIc} were decreased by 15 and 11 percent, respectively, when temperature was increased from 25 to 1316 °C. However, this decrease was marginal, as can be seen in a summary of K_{Ic} as a function of temperature in figure 6, in which the K_{Ic} data previously determined[11] at 25 and 800 °C by the SEVNB method were included with the current data. K_{Ic} remains statistically invariable with an average of K_{Ic} = 1.0±0.1 MPa $\sqrt{m}$, regardless of test temperature up to 1316 °C. The same would be true for K_{IIc} (=0.69 MPa $\sqrt{m}$) as depicted in the figure, notwithstanding the lack of intermediate-temperature data. The insensitivity of K_{Ic} to temperature was also observed in a similar but dense (hot-pressed) 10 mol% yttria-stabilized zirconia (10-YSZ) in which fracture toughness of the material—evaluated in air by the same SEVNB method—was almost unchanged (K_{Ic} = 1.6-1.8 MPa $\sqrt{m}$) from 25 to 1000 °C.[9]

Figure 7 shows typical examples of crack propagation with different mixities ranging from pure mode II ($K_I/K_{II} = 0$) to pure mode I ($K_I/K_{II} = \infty$). The angle of crack propagation θ_c was defined as an angle of the crack plane propagated with respect to the original precrack plane. The direction of crack plane propagated was in most cases straight with some exceptions such as tortuous or not-straight paths. The angle of crack

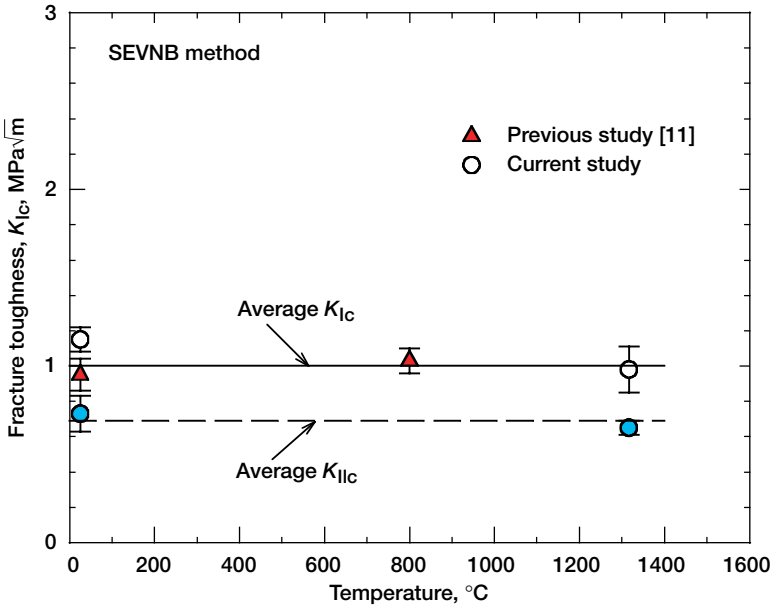

Figure 6.—Fracture toughnesses of K_{Ic} and K_{IIc} as a function of temperature for plasma-sprayed ZrO_2-8 wt% Y_2O_3 thermal barrier coatings. The previous K_{Ic} data[11] were included. Error bars represent ±1.0 standard deviation.

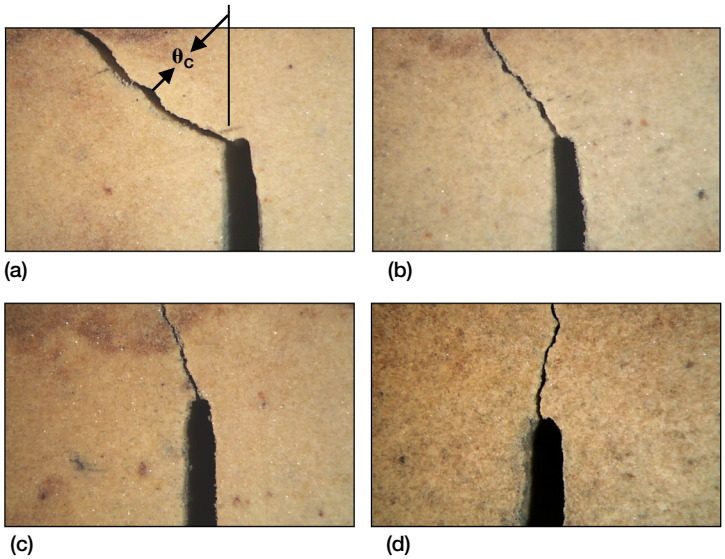

Figure 7.—Typical examples of specimens showing angles of crack propagation with respect to K_I/K_{II} of plasma-sprayed ZrO_2-8 wt% Y_2O_3 thermal barrier coatings: (a) pure mode II; K_I/K_{II} = 0, (b) K_I/K_{II} = 2.7, (c) K_I/K_{II} = 5.5, and (d) pure mode I; K_I/K_{II} = ∞.

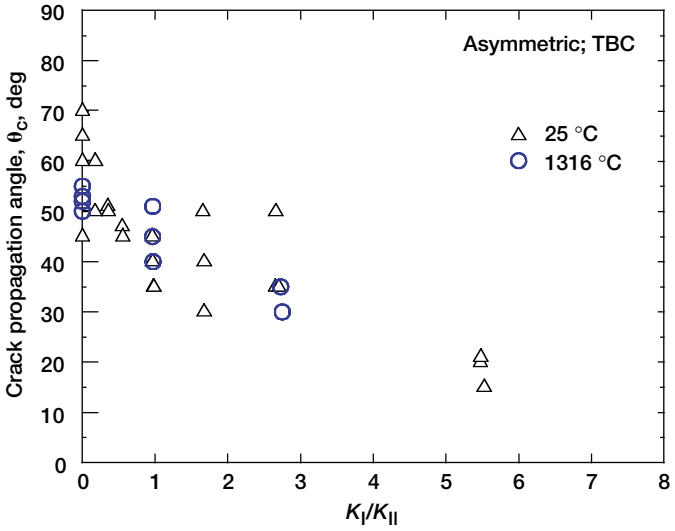

Figure 8.—Crack propagation angles as function of K_I/K_{II} of plasma-sprayed ZrO_2-8 wt% Y_2O_3 thermal barrier coatings determined in asymmetric four-point flexure at both 25 and 1316 °C in air.

propagation was greatest in pure mode II, and decreased with increasing K_I/K_{II} reaching to $\theta_c = 0$ in pure mode I. A summary of experimental data on the angle of crack propagation as a function of K_I/K_{II} determined at both 25 and 1316 °C is depicted in figure 8. The overall trend of the angle of crack propagation was that θ_c initially decreased quickly with increasing K_I/K_{II} and then decreased monotonically at $K_I/K_{II} > 3$. No significant difference in θ_c between 25 and 1316 °C was observed. It is noted that the scatter in θ_c, for example, $\theta_c = 45$ to 70° at $K_I/K_{II} = 0$ (pure mode II), seemed more appreciable in the coating material than in dense advanced ceramics,[22] which exhibited a typical scatter of about 15°.

Analysis of fracture surfaces revealed no explicit difference in the fracture morphology of the pure mode I, mixed-mode, or pure mode II specimens. However, it should be mentioned that unlike dense ceramics the coating material has provided a challenging subject on fractography because of its unique open and microcracked platelet microstructure. The origin or nature of strength-controlling flaws in the coating material has rarely been identified with any traditional means of fractography (optical and/or SEM) that would be otherwise sufficient for the case of dense ceramics.[12] An improved means of fractography is required to better distinguish fracture morphologies in response to different modes of fracture of the coating material.

3.2. Consideration of Mixed-Mode Fracture Criteria

3.2.1. Considered Criteria

As shown from the crack propagation angles in figure 8, mixed-mode fracture does not take place in the same plane as the original crack. This noncoplanar crack propagation requires different fracture criteria, typically a combination of the driving forces K_I and K_{II} together with K_{Ic} and K_{IIc}. The mixed-mode fracture criteria for an isotropic, homogeneous material can be broadly categorized in four areas and will be briefly described then compared with experimental results.

3.2.1a. Maximum Principal Stress Criterion.[24] This criterion assumes that a crack at instability propagates in the direction normal to the maximum principal stress direction. The instability condition is given by the following relationship:

$$K_{Ic} - K_I \cos^3\frac{\theta_c}{2} + 3K_{II}\cos^2\frac{\theta_c}{2}\sin\frac{\theta_c}{2} = 0 \tag{10}$$

The angle of crack propagation θ_c is a function of K_I/K_{II} and is given by

$$\theta_c = 2\tan^{-1}\left\{\frac{K_I}{4K_{II}} \pm \frac{1}{4}\left[\left(\frac{K_I}{K_{II}}\right)^2 + 8\right]^{1/2}\right\} \tag{11}$$

In case of pure mode II, the following relations can be obtained from Eqs. (10) and (11):

$$\theta_c = 70.53°, \quad \frac{K_{IIc}}{K_{Ic}} = 0.8662 \tag{12}$$

3.2.1b. Minimum Strain Energy Density Criterion.[25] This criterion assumes that crack propagation would take place in the direction along which the strain energy density is minimum. This assumption gives rise to the following mixed-mode fracture criterion

$$K_{Ic}^2 - \frac{1}{2(\kappa-1)}[a_{11}K_I^2 + 2a_{12}K_IK_{II} + a_{22}K_{II}^2] = 0 \tag{13}$$

where

$$a_{11} = (1+\cos\theta_c)(\kappa - \cos\theta_c)$$
$$a_{12} = \sin\theta_c\,(2\cos\theta_c - \kappa + 1)$$
$$a_{22} = (\kappa+1)(1-\cos\theta_c) + (1+\cos\theta_c)(3\cos\theta_c - 1)$$

with

$$\kappa = 3–4\nu \quad \text{for plain strain}$$

$$\kappa = (3-\nu)/(1+\nu) \quad \text{for plain stress}$$

where ν is Poisson's ratio. The angle of crack propagation, θ_c, is given by

$$(\kappa-1)\sin\left(\theta_c - 2\tan^{-1}\frac{K_I}{K_{II}}\right) - 2\sin\left[2\left(\theta_c - \tan^{-1}\frac{K_I}{K_{II}}\right)\right] - \sin 2\theta_c = 0 \tag{14}$$

In case of pure mode II, the following relations can be obtained from Eqs. (13) and (14):

$$\theta_c = \cos^{-1}\left(\frac{\kappa-1}{6}\right), \quad \frac{K_{IIc}}{K_{Ic}} = \left[\frac{2(\kappa-1)}{a_{22}}\right]^{1/2} \tag{15}$$

3.2.1c. Maximum Energy Release Rate Criterion. This criterion assumes that a crack with an infinitesimally small kink at an arbitrary direction propagates in the direction along the maximum strain energy release rate.[26, 29] Many investigators keeps that the strain energy release rate, G, can be expressed in terms of K_I and K_{II} as follows:

$$G = c_{11}K_I^2 + c_{12}K_IK_{II} + c_{22}K_{II}^2 \tag{16}$$

where c_{11}, c_{12}, and c_{22} are coefficients. Hyashi and Nemeat-Nasser[28] determined numerically the coefficients and the direction of maximum G as a function of K_I/K_{II}. Palaniswamy and Knauss[27] proposed an approximated mixed-mode fracture criterion on the maximum energy release rate as follows (that was also used by Suresh et al.[15])

$$\frac{K_I}{K_{Ic}} + \frac{3}{2}\left(\frac{K_{II}}{K_{Ic}}\right)^2 = 1 \tag{17}$$

where for pure mode II the approximation leads to

$$\theta_c = 77.4°, \quad \frac{K_{IIc}}{K_{Ic}} = 0.817 \tag{18}$$

The fracture criterion and the crack propagation angle on the maximum G were used based on Eqs. (16) and (17) in this work.

3.2.1d. Empirical Criterion.[30, 31] The empirical fracture criterion can be expressed by the following generalized, simplified form

$$\left(\frac{K_I}{K_{Ic}}\right)^p + \left(\frac{K_{II}}{\gamma K_{Ic}}\right)^q = 1 \tag{19}$$

where p and q are parameters (typically p,q = 1–2) to be determined from experimental data through a curve fitting, and

$$\gamma = \frac{K_{IIc}}{K_{Ic}} \tag{20}$$

with $0<\gamma<2$, an experimentally determined value. Despite the lack of its theoretical frame work in some cases, the empirical fracture criterion can still provide a much simplified representation (as database, too) of mixed-mode behavior of a material particularly when other (preceding) fracture criteria do not describe reasonably well the actual material's behavior under mixed mode. The maximum G criterion (Eq. 15) or the coplanar crack propagation criterion,[32] in fact, is one particular type of the empirical fracture criterion in its form.

3.2.2. Comparison with Experiment

Figure 9 compares the afore-reviewed four different mixed-mode fracture criteria with the experimental data (that were presented in fig. 5), where K_{II} normalized with respect to K_{Ic}, K_{II}/K_{Ic}, was plotted as a function of K_I/K_{Ic} for both 25 and 1316 °C data. The prediction for the minimum strain energy density criterion was made using a value of $\nu = 0.2$. Neither the maximum principal stress nor the minimum strain energy density nor the maximum energy release rate criterion was in reasonable agreement with the

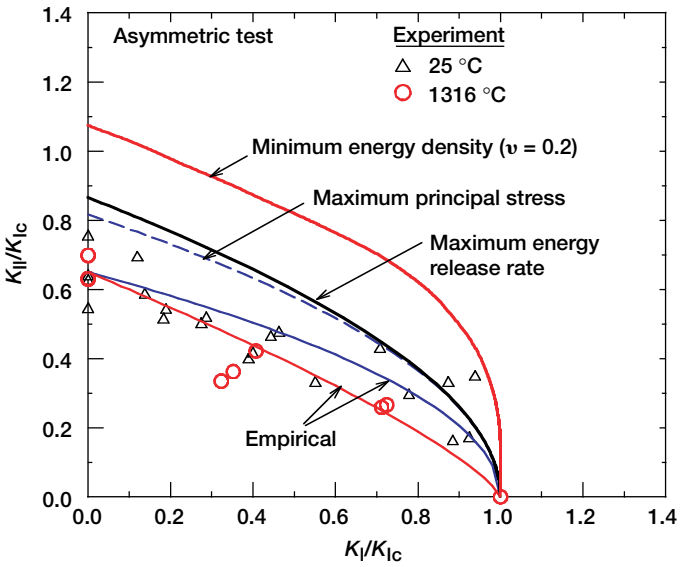

Figure 9.—Plots of K_{II}/K_{Ic} as a function of K_I/K_{Ic} for mixed-mode fracture criteria and experimental data determined for plasma-sprayed ZrO_2-8 wt% Y_2O_3 thermal barrier coatings. υ is Poisson's ratio.

experimental data. Only the empirical criterion was in good agreement with both ambient and elevated-temperature data, resulting in the following parameters:

$$p = 1; q = 2; \gamma = 0.65 \quad \text{for 25 °C}$$
$$p = 1; q = 1.3; \gamma = 0.65 \quad \text{for 1316 °C} \tag{21}$$

Previous studies on dense ceramics such as silicon nitrides and alumina[22] and ceria-doped ziconia[23] showed that the minimum strain energy density criterion resulted in best agreement among the mixed-mode criteria mentioned above, as that was the case in another study of alumina by Suresh et al. as well.[15] Hence, there exists a remarkable contrast in mixed-mode behavior between the dense and the porous TBC ceramics. The unique nature of the coating material—possessing porosity, microcracks, and platelet microstructure—might have been responsible for the ability to distinguish its unique mixed-mode fracture pattern, as this is not the case for dense ceramics. As also seen from figure 9, the three mixed-mode fracture criteria—the maximum principal stress, minimum strain energy density, and maximum energy release rate criteria—predict the values of K_{IIc}/K_{Ic} = 0.8 to 1.1. The poor agreement with these three fracture criteria was, therefore, due to the lower values of K_{IIc}/K_{Ic} that were around 0.65 for the coating material at both temperatures. Hence, the value of K_{IIc}/K_{Ic} is the parameter with the largest influence on the degree of agreement with the prediction of the fracture pattern. In case of $K_{IIc}/K_{Ic} \approx 1$, statistically reasonable agreement would be found in any of the major mixed-mode fracture criteria mentioned. The dense ceramics examined in previous studies[22, 23] all exhibited a value close to $K_{IIc}/K_{Ic} \approx 1$. Comparison of K_{IIc}/K_{Ic} among other brittle materials will be presented and discussed below.

The data on crack propagation angle shown in figure 8 were compared with the predictions made with the three mixed-mode fracture criteria, and the results are presented in figure 10. The minimum strain energy density criterion overall seemed to yield a better prediction compared with the other two criteria. However, because of somewhat significant scatter in θ_c as well as little difference in prediction between the criteria, it is difficult to state which criterion gives the best agreement with the experimental data. Note that a significant discrepancy was found particularly in the region close to pure mode II, e.g., $K_I/K_{II} < 1$. This discrepancy predominant in the region of $K_I/K_{II} < 1$ was also observed in the previous studies with silicon nitrides and alumina[22] and other grade alumina by Suresh et al.[15] By contrast, this discrepancy seemingly unique in ceramics was not found in amorphous glassy polymer PMMA (polymethylmethacrylate) mixed-mode tested in either asymmetric four-point flexure[23] or uniaxial tension[25] configuration. A good agreement of propagation angle with the fracture criteria (as well as little scatter in θ_c) in a wide range of K_I/K_{II} close to pure mode II was also found in steel tested in asymmetric four-point flexure at –196 °C to induce brittle fracture.[33]

As previously mentioned, the overall locus of mixed-mode fracture (in K_{II} versus K_I, or K_{II}/K_{Ic} versus K_I/K_{Ic} relation) is mainly controlled by the value of K_{IIc}/K_{Ic}; hence, the ratio of mode II fracture toughness to mode I fracture toughness is a very important measure of a material in terms of its response to mixed-mode fracture. With this in mind,

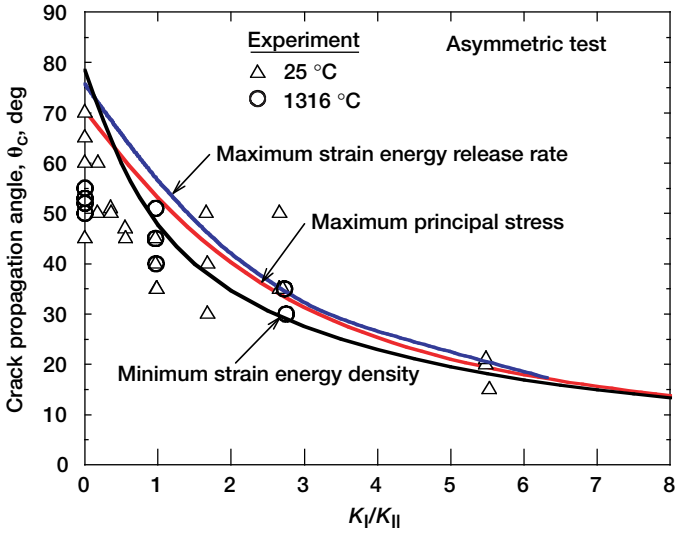

Figure 10.—Plots of crack propagation angle as a function of K_I/K_{II} for mixed-mode fracture criteria and experimental data determined for plasma-sprayed ZrO_2-8 wt% Y_2O_3 thermal barrier coatings.

a summary of data on K_{IIc}/K_{Ic} for various brittle materials compiled by Munz and Fett[31] as well as data on dense ceramics from previous studies[22, 23] was used and compared with the TBC data obtained in this work, as shown in figure 11. The values of K_{IIc}/K_{Ic} for the dense ceramics two silicon nitrides (one with fine and one, elongated grains), coarse grained alumina,[22] and ceria-doped tetragonal zirconia polycrystal (Ce-TZP),[23] all tested in asymmetric four-point flexure using *naturally* sharp precracks, are invariably around $K_{IIc}/K_{Ic} = 1$ and are much greater than those of the TBC ($K_{IIc}/K_{Ic} \approx 0.65$). Except for this comparison, a large variation of K_{IIc}/K_{Ic} varying from 0.6 to 2.0 is noted depending on materials, test specimens, notch or initial crack preparations, and even investigators, etc. As a result of this significant variation, a reasonably unified trend on the value of K_{IIc}/K_{Ic} cannot be made for the materials provided. However, it should be noted that the value of K_{IIc}/K_{Ic} for the TBC evaluated in this work is still at the lower end of the data pool. One thing to note is that test technique must be technically sound, particularly in the areas of specimen configuration and precrack preparation. A diametral compression technique, for example, would be in danger to overestimate greater K_{IIc} as a result of frictional constraint between the two crack faces by the existence of compressive stress therein.[22] Use of sharp precracks using an appropriate method such as single edge precrack beam (SEPB) method[14] or SEVNB method as used in this work is also crucially important to obtain as accurate fracture toughness as possible.

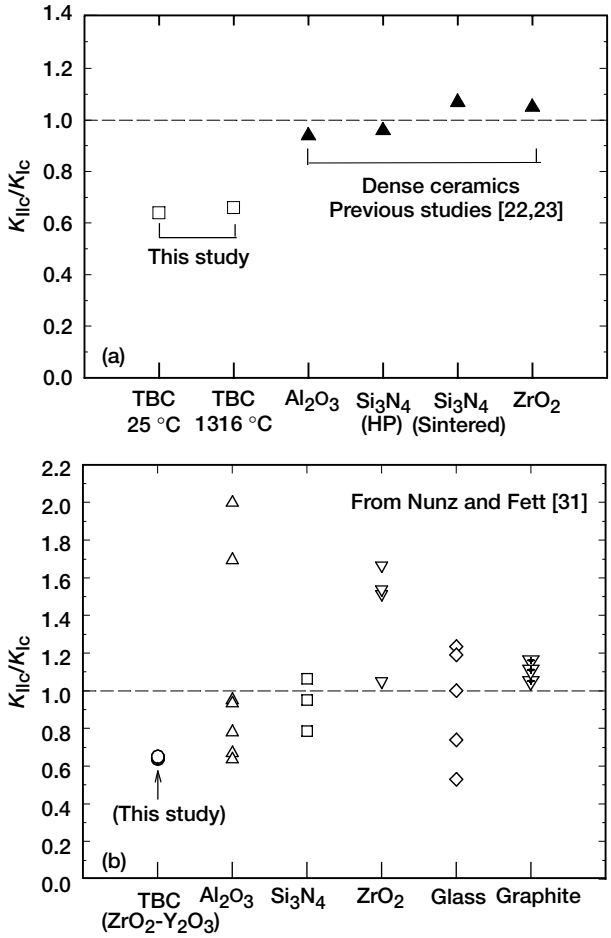

Figure 11.—Comparisons of K_{IIc}/K_{Ic} of plasma-sprayed ZrO_2-8 wt% Y_2O_3 thermal barrier coatings with other advanced monolithic ceramics and brittle materials at ambient temperature. (a) Comparison with previous studies[22,23]. (b) Comparison with data compiled by Munz and Fett[31].

3.3. Effect of Directionality

To determine a possible effect of the material's directionality on fracture toughness, mode I fracture toughness testing for the coating material was performed by the DCB method in the direction perpendicular to the plasma-sprayed direction, as mentioned in the Experimental section. The value of fracture toughness was found to be K_{Ic} = 1.04±0.05 MPa $\sqrt{m}$. This value of K_{Ic} was very similar to that of K_{Ic} = 1.15±0.07 MPa $\sqrt{m}$ determined in the direction parallel to plasma-spraying direction. Hence, the directionality of the coating material in response to mode I fracture toughness was insignificant. The previous

studies showed that even the tensile strength of the coatings with different vintages was almost independent whether the plasma-spraying direction which was either perpendicular or parallel. Therefore, a notion that mechanical properties of TBC would be *strongly* dependent on the direction of plasma spraying may not be supported and generalized, based on the fracture toughness testing in this study and the strength testing in previous studies.[12]

3.4. Effect of Sintering

Figure 12 shows the results of mode I fracture toughness testing for the coating material annealed at 1316 °C in air with annealing times ranging from t = 0 (as-sprayed) to 500 h. Fracture toughness increased significantly at t = 5 h, increased monotonically to t = 100 h, and then reached a plateau at t = 500 h with a value of K_{Ic} = 2.6±0.2 MPa$\sqrt{m}$, about a 120 percent increase from t = 0. This increase in K_{Ic} was attributed to a sintering effect.[6] Figure 13 shows typical fracture surfaces of specimens tested, subjected to annealing for t = 0 and 100 h. The sintering effect was manifest by the evidence of significant grain growth for the specimen annealed for t = 100 h. It has been shown that sintering gives rise to an increase not only in fracture toughness but in elastic modulus, strength, and thermal conductivity of the coating material.[34, 12, 6] Although not performed in this work, it is expected that K_{IIc} in response to sintering would follow a trend similar to K_{Ic}. Therefore, evaluation of K_{IIc} as a function of annealing time at 1316 °C is an immediate task for future study. Since a change in mechanical properties (and physical properties as well) would occur inevitably upon sintering, particularly in a short period of

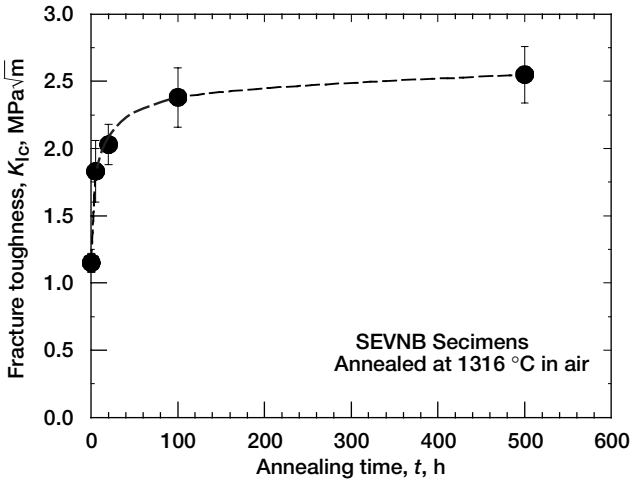

Figure 12.—Result of fracture toughness as a function of annealing time for plasma-sprayed ZrO_2-8 wt% Y_2O_3 thermal barrier coatings annealed at 1316 °C in air.

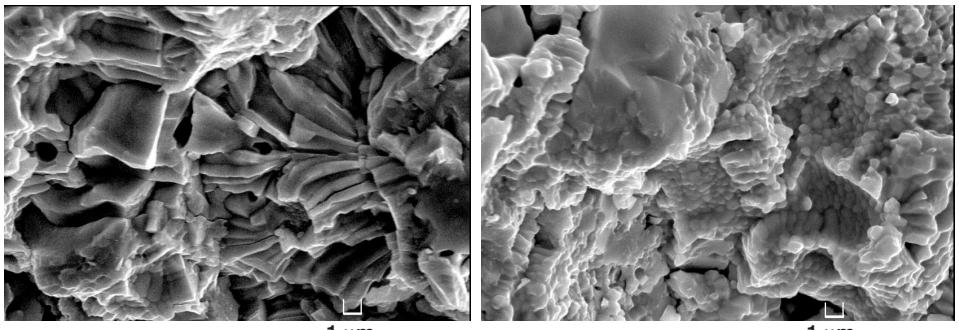

Figure 13.—Comparison of fracture surfaces of fracture toughness-tested specimens of plasma-sprayed ZrO_2-8 wt% Y_2O_3 thermal barrier coatings. (a) As-sprayed. (b) Annealed in air at 1316 °C for 100 h.

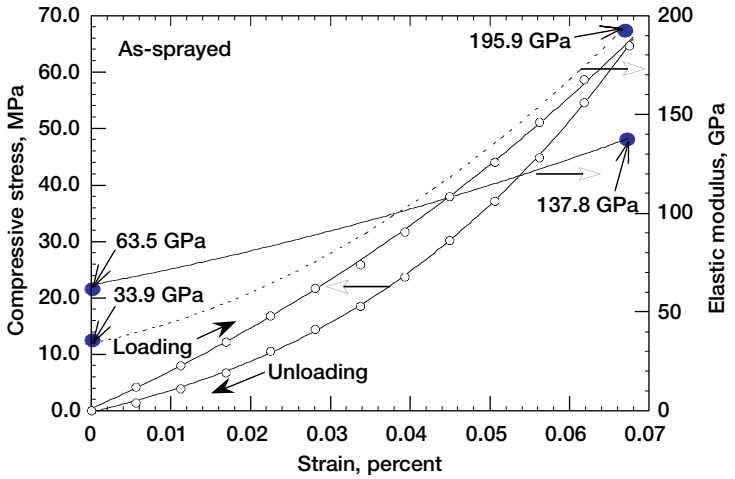

Figure 14.—Typical stress-strain curve for plasma-sprayed ZrO_2-8 wt% Y_2O_3 thermal barrier coatings in compression[11].

time, a continuous use of as-sprayed mechanical data in elevated-temperature applications would give an over-conservative estimate, leading to erroneous results in reliability and/or life predictions of components.

3.5. Other Considerations

Finally, it should be mentioned that the coating material has shown nonlinearity and hysteresis in its stress-strain relation, irrespective of loading configuration: tension, uniaxial or biaxial flexure, or compression.[12] A typical result showing such nonlinearity and hysteresis exhibited in compression by the as-sprayed ZrO_2-Y_2O_3 coatings is presented in figure 14. This nonlinearity in constitutive relation was due to the coatings'

unique microstructure (porosity, microcracks, and platelets) and diminished upon annealing to a degree depending on annealing time and temperature. A question arises as to whether linear elastic fracture mechanics (LEFM) approach could be applicable to this nonlinear, elastic, as-sprayed coating material. The degree of nonlinearity was more significant when the level of applied stress was increased. In most cases, however, fracture force employed in fracture toughness testing was relatively low (with about one tenth of the peak force in figure 14), and in this case the nonlinearity became negligibly small. As a result, an LEFM approach (a continuum approach as well) would be justified at least in fracture toughness testing for the as-sprayed coating material.

4. CONCLUSIONS

A full range of mixed-mode fracture behavior covering mode I and mode II for plasma-sprayed ZrO_2-8 wt% Y_2O_3 thermal barrier coating was determined in air at 25 and 1316 °C in asymmetric four-point flexure in conjunction with the single edge v-notched beam (SEVNB) method. The following conclusions were made:

1. The mode I fracture toughness was found to be K_{Ic} = 1.15±0.07 and 0.98±0.13 MPa$\sqrt{m}$, respectively, at 25 and 1316 °C. The respective mode II fracture toughness was K_{IIc} = 0.73±0.10 and 0.65±0.04 MPa$\sqrt{m}$. Hence, the coating material exhibited an insignificant difference in either K_{Ic} or K_{IIc} between 25 and 1316 °C, whereas it exhibited noticeable difference between K_{Ic} and K_{IIc}, resulting in K_{IIc}/K_{Ic} = 0.65 at both temperatures.
2. The empirical mixed-mode fracture criterion was in best agreement with the coating's mixed-mode fracture behavior among the four mixed-mode fracture theories considered. The angle of crack propagation was in reasonable agreement with the minimum strain energy density criterion.
3. The mode I fracture toughness of the coating material at 25 °C was almost irrespective of the plane either parallel (typical) or perpendicular to plasma spraying direction so that the coating's directionality in response to K_{Ic} was insensitive.
4. Sintering at 1316 °C in air showed a significant influence on mode I fracture toughness, giving rise to an increase in K_{Ic} at the plateau region by 120 percent when the coatings were annealed for the duration of 500 h.

5. REFERENCES

1. R. A. Miller, "Current Status of Thermal Barrier Coatings—An Overview," *Surface and Coating Technology*, **30**, 1–11 (1987).
2. R. A. Miller, "Thermal Barrier Coatings for Aircraft Engines—History and Direction," pp. 17–34 in NASA CP–3312 (Ed. W.J. Brindley), National Aeronautics and Space Administration, Glenn Research Center, Cleveland, OH (1995).
3. T. M. Yonushonis, "Thick Thermal Barrier Coatings for Diesel Components," NASA CR–187111, National Aeronautics and Space Administration, Glenn Research Center, Cleveland, OH (1991).

4. Y. C. Tsui, T. W. Clyne, *Proc. 9th Nat. Thermal Spray Conf*., Cincinnati, OH (1996).
5. L. L. Shaw, B. Barber, E. H. Jordan, and M. Gell, *Scr. Mater*., **39** 1427–1434 (1998).
6. G. Thurn, G. A. Schneider, H. A. Bahr, and F. Aldinger, "Toughness Anisotropy and Behavior of Plasma Sprayed ZrO_2 thermal Barrier Coatings," *Surf. Coat. Tech*., **123**, 147–158 (2000).
7. K. F. Wesling, D. F. Socie, and B. Beardsley, "Fatigue of Thick Thermal Barrier Coatings," *J. Am. Ceram. Soc*., **77**[7] 1863–1868 (1994).
8. P. J. Callus and C. C. Berndt, "Relationship between the Mode II Fracture Toughness and Microstructure of Thermal Spray Coatings," *Surf. Coat. Tech*., **114,** 114–128 (1999).
9. S. R. Choi and N. P. Bansal, "Strength and Fracture Toughness of Zirconia/Alumina Composites for Solid Oxide Fuel Cells," *Ceram. Eng. Sci. Proc*., **23**[3] 741–750 (2002); "Processing and Mechanical Properties of Various Zirconia/Alumina Composites for Fuel Cells Applications," NASA/TM—2002-211580, National Aeronautics and Space Administration, Glenn Research Center, Cleveland, OH (2002); also presented at CIMTEC 2002 Conference, paper no. G1:P03 (to be published in the proceedings), June 14–18, 2002, Florence, Italy.
10. D-M. Zhu and R. A. Miller, "Influence of High Cycle Thermal Loads on Thermal fatigue Behavior of Thick Thermal Barrier Coatings," NASA Technical paper 3676 (also in Army Laboratory Technical Report ARL–TR–1341), National Aeronautics and Space Administration, Glenn Research Center, Cleveland, OH (1997).
11. S. R. Choi, D-M. Zhu, and R. A. Miller, "High-Temperature Slow Crack Growth, Fracture Toughness and Room-Temperature Deformation Behavior of Plasma-Sprayed ZrO_2-8 wt% Y_2O_3," *Ceram. Eng. Sci. Proc*., **19**[4] 293–301 (1998).
12. S. R. Choi, D-M. Zhu, and R. A. Miller, "Deformation and Strength Behavior of Plasma-Sprayed ZrO_2-8 wt% Y_2O_3 Thermal Barrier Coatings in Biaxial Flexure and Trans-Thickness Tension," *Ceram. Eng. Sci. Proc*., **21**[4] 653–661 (2000).
13. J. Kübler, (a) "Fracture Toughness of Ceramics Using the SEVNB Method: Preliminary Results," *Ceram. Eng. Sci. Proc*., **18**[4] 155–162 (1997); (b) "Fracture Toughness of Ceramics Using the SEVNB Method; Round Robin," VAMAS Report No. 37, EMPA, Swiss Federal Laboratories for Materials Testing & Research, Dübendorf, Switzerland (1999).
14. ASTM C 1421 "Test Method for Determination of Fracture Toughness of Advanced Ceramics at Ambient Temperature," *Annual Book of ASTM Standards*, Vol. 15.01, American Society for Testing and materials, West Conshohocken, PA (2002).
15. S. Suresh, C. F. Shih, A. Morrone, and N. P. O'Dowd, "Mixed-Mode Fracture Toughness of Ceramic Materials," J. *Am. Ceram. Soc*., **73**[5] 1257–1267 (1990).
16. K. J. Wang, H. C. Lin, and K. Hua, "Calculation of Stress Intensity Factors for Combined Mode Bend Specimens," pp. 123–133 in *Advances in Research on the Strength and Fracture of Materials*, Vol. 4, Edited by M. D. R. Taplin, ICF4, Waterloo, Canada (1977).
17. M. Y. He and J. W. Hutchinson, "Asymmetric Four-Point Crack Specimen," *J. Appl. Mech*., **67**, 207–209 (2000).

18. Y. Murakami (ed.), Stress Intensity Factors Handbook, Vol. 1, p. 16, Pergamon Press, New York (1987).
19. J. E. Srawley and B. Gross, "Side-Cracked Plates Subjected to Combined Direct and Bending Forces," pp. 559–579 in *Cracks and Fracture*, ASTM STP 601, American Society for Testing and Materials, Philadelphia (1976).
20. T. M. Maccagno and J. F. Knott, "The Fracture Behavior of PMMA in Mixed Modes I and II," *Eng. Fract. Mech*., **34**[1] 65–86 (1989).
21. D. K. Shetty, A. R. Rosenfield, and W. H. Duckworth, "Mixed-Mode Fracture of Ceramics in Diametral Compression," *J. Am. Ceram. Soc*., **69**[6] 437–443 (1986).
22. V. Tikare and S. R. Choi, "Combined Mode I and Mode II Fracture of Monolithic Ceramics," *J. Am. Ceram. Soc*., **76**[9] 2265–2272 (1993).
23. V. Tikare and S. R. Choi, "Combined Mode I-Mode II Fracture of 12-mol-%-Ceria-Doped Tetragonal Zirconia Polycrystalline Ceramic," *J. Am. Ceram. Soc*., **80**[6] 1624–1626 (1997).
24. F. Erdogan and G. C. Sih, "On the Crack Extension in Plates under Plane Loading and Transverse Shear," *J. Basic Eng*., **85**, 519–527 (1963)
25. G. C. Sih, "Strain-Energy-Density Factor Applied to Mixed Mode Crack Problems," *Int. J. Fracture*, **10**[3] 305–321 (1974).
26. R. J. Niusmer, "An Energy Release Rate Criterion for Mixed Mode Fracture," *Int. J. Fracture,* **10**[3] 305–321 (1974)
27. K. Palaniswamy and W. G. Knauss, "On the Problem of Crack Extension in Brittle Solids under General Loading," pp. 87–148 in *Mechanics Today*, Vol. 4, Edited by S. Nemat-Nasser, Pergamon Press, New York (1978).
28. K. Hyashi and S. Nemat-Nasser, " " *J. Appl. Mech*., **48**, 520–524 (1981).
29. Y. Ueda, K. Ikeda, T. Yoa, and M. Aoki, "Characteristics of Brittle Fracture under General Combined Modes Including Those under Biaxial Tensile Loads," *Eng. Fract. Mech*., **18**[6] 1131–1158 (1983).
30. D. K. Shetty, "Mixed-Mode Fracture Criteria for Reliability Analysis and Design with Structural Ceramics," *J. Eng.Gas Turbine Power*, **109**[7] 282–289 (1987).
31. D. Munz and T. Fett, Ceramics, pp. 45–49, Springer-Verlag, Berlin, Germany (1999).
32. P. C. Paris and G. C. Sih, "Stress Analysis of Cracks," ASTM ATP 381, pp. 30–81, American Society for Testing and Materials, Philadelphia, PA, 1965.
33. T. M. Maccagno and J. F. Knott, "The Low Temperature Brittle Fracture Behavior of Steel in Mixed Modes I and II," *Eng. Fract. Mech*., **38**[2–3] 111–128 (1991).
34. D-Z. Zhu and R. A. Miller, "Thermal Conductivity and Elastic Modulus Evolution of Thermal Barrier Coatings under High Heat Flux Conditions," NASA/TM—1999-209069, National Aeronautics and Space Administration, Glenn Research Center, Cleveland, OH (1999).

REPORT DOCUMENTATION PAGE

Form Approved
OMB No. 0704-0188

1. AGENCY USE ONLY (*Leave blank*)	2. REPORT DATE	3. REPORT TYPE AND DATES COVERED
	March 2003	Technical Memorandum

4. TITLE AND SUBTITLE

Mode I, Mode II, and Mixed-Mode Fracture of Plasma-Sprayed Thermal Barrier Coatings at Ambient and Elevated Temperatures

5. FUNDING NUMBERS

WBS–22–714–04–30

6. AUTHOR(S)

Sung R. Choi, Dongming Zhu, and Robert A. Miller

7. PERFORMING ORGANIZATION NAME(S) AND ADDRESS(ES)

National Aeronautics and Space Administration
John H. Glenn Research Center at Lewis Field
Cleveland, Ohio 44135–3191

8. PERFORMING ORGANIZATION REPORT NUMBER

E–13787

9. SPONSORING/MONITORING AGENCY NAME(S) AND ADDRESS(ES)

National Aeronautics and Space Administration
Washington, DC 20546–0001

10. SPONSORING/MONITORING AGENCY REPORT NUMBER

NASA TM—2003-212185

11. SUPPLEMENTARY NOTES

Prepared for the Eighth International Symposium on Fracture Mechanics of Ceramics sponsored by the University of Houston, Houston, Texas, February 25–28, 2003. Sung R. Choi, Ohio Aerospace Institute, Brook Park, Ohio 44142; Dongming Zhu, U.S. Army Research Laboratory, NASA Glenn Research Center; Robert A. Miller, NASA Glenn Research Center. Responsible person, Sung R. Choi, organization code 5920, 216–433–8366.

12a. DISTRIBUTION/AVAILABILITY STATEMENT

Unclassified - Unlimited
Subject Category: 07 Distribution: Nonstandard

Available electronically at http://gltrs.grc.nasa.gov

This publication is available from the NASA Center for AeroSpace Information, 301–621–0390.

12b. DISTRIBUTION CODE

13. ABSTRACT ***(Maximum 200 words)***

The mixed-mode fracture behavior of plasma-sprayed ZrO_2-8 wt% Y_2O_3 thermal barrier coatings was determined in air at 25 and 1316 °C in asymmetric four-point flexure with single edge v-notched beam (SEVNB) test specimens. The mode I fracture toughness was found to be K_{Ic} = 1.15 ± 0.07 and 0.98 ± 0.13 MPa $\sqrt{m}$, respectively, at 25 and 1316 °C. The respective mode II fracture toughness values were K_{IIc} = 0.73 ± 0.10 and 0.65 ± 0.04 MPa $\sqrt{m}$. Hence, there was an insignificant difference in either K_{Ic} or K_{IIc} between 25 and 1316 °C for the coating material, whereas there was a noticeable distinction between K_{Ic} and K_{IIc}, resulting in K_{IIc}/K_{Ic} = 0.65 at both temperatures. The empirical mixed-mode fracture criterion best described the coatings' mixed-mode fracture behavior among the four mixed-mode fracture theories considered. The angle of crack propagation was in reasonable agreement with the minimum strain energy density criterion. The effect of the directionality of the coating material in on K_{Ic} was observed to be insignificant, while its sintering effect at 1316 °C on K_{Ic} was significant.

14. SUBJECT TERMS

Thermal barrier coatings; Plasma-sprayed ZrO_2–Y_2O_3; Mixed mode fracture; Fracture toughness; Fracture toughness testing; Elevated-temperature testing

15. NUMBER OF PAGES

28

16. PRICE CODE

17. SECURITY CLASSIFICATION OF REPORT	18. SECURITY CLASSIFICATION OF THIS PAGE	19. SECURITY CLASSIFICATION OF ABSTRACT	20. LIMITATION OF ABSTRACT
Unclassified	Unclassified	Unclassified	